Journal of the Korean Physical Society, Vol. 55, No. 6, December 2009, pp. 2560∼2565

Simulation of Reentrant Wave Dynamics in Cardiac Tissue According to the Severity of Fibrosis

Ki Moo Lim, Seung Yoon Choi, Soon Sung Kwon and Eun Bo Shim*

Department of Mechanical & Biomedical Engineering, Kangwon National University, Chuncheon 200-701

(Received 15 June 2009, in final form 19 August 2009)

This study investigated the spiral wave dynamics in cardiac tissue according to the severity of fibrosis in the hypertrophic human ventricle by simulating propagation of the electric wave. We used a model of the human ventricular cell to describe the cellular electrophysiology and a two-dimensional monodomain method to compute the electric wave propagation in ventricular tissue using finite element approximation. To delineate the effect of fibrosis on the wave dynamics, a model of hypertrophic cardiac tissue with randomly distributed fibroblasts was simulated. The electrical conductivity of the fibroblasts was estimated from the experimental data. In the fibrotic cardiac tissue, we generated a reentrant wave and predicted its dynamic variation according to the severity of fibrosis. Compared to the reentrant wave in normal tissue, a conduction delay was observed in the fibrotic tissue. Furthermore, one spiral wave broke into several waves when fibroblasts constituted 40 % of the tissue, causing cardiac fibrillation.

PACS numbers: 87.19.Hh
Keywords: Fibrosis, Reentrant wave, Simulation study
DOI: 10.3938/jkps.55.2560

I. INTRODUCTION

In cardiac tissue, reentrant waves are generated from the instability of electrical wave propagation, which constitutes the major mechanism underlying fatal arrhythmias, such as tachycardia or fibrillation [1]. Stationary or drifting reentrant wave patterns in cardiac tissue are closely related to its physiological properties, and the wave patterns in diseased tissue are critical for the generation of arrhythmic chaos or fibrillation, which results in the sudden cardiac death of patients [2,3].

Extensively investigated hypotheses to explain ventricular fibrillation are related to factors such as short-term cardiac memory, electrotonic interactions between cells, conduction velocity restitution, action potential duration restitution, and fibrotic tissue [4–9]. Cherry and Fenton [10] demonstrated the effect of electrotonic interactions between cells and conduction velocity restitution on reentrant wave dynamics. The action potential duration restitution hypothesis has stimulated a large number of experimental studies. The hypothesis states that if the action potential duration (APD) restitution curve has a maximum slope steeper than 1, it will lead to APD alternans, which can result in the fragmentation of a spiral wave, leading to fibrillation [8,11].

*Corresponding Author: ebshim@kangwon.ac.kr;
Tel: +82-33-250-6318; Fax: +82-33-242-6013

In addition to experimental work, many computational studies have examined the mechanism of reentrant waves and the underlying cellular phenomena [12–14]. Fenton *et al.* provided multiple mechanisms for reentrant wave breakup [15]. Using a realistic ventricular geometry, Berenfeld and Jalife investigated the interaction of ventricular tissue with Purkinje fibers in reentrant wave dynamics [16]. ten Tusscher *et al.* [17] proved the restitution hypothesis using a computational model of human ventricular tissue.

Despite several computational studies on arrhythmia, the effect of cardiac fibrosis on reentrant wave dynamics has not been analyzed thoroughly. In general, the progressive development of heart failure is accompanied by hypertrophy or ventricular wall thickening due to the increased afterload [18,19]. In this setting, some of the cardiac tissue is partially replaced by fibroblasts, which are not connected to normal cardiac cells via gap junctions, inhibiting the conduction of electric waves in cardiac tissue. This, in turn, can induce chaotic electric waves, resulting in tachycardia or fibrillation.

In this study, we examined the effect of fibrosis in hypertrophic ventricle tissue on the propagation of the action potential in ventricular tissue by using a computational method. The human ventricular cell model proposed by ten Tusscher *et al.* [20] (the TNNP model) was adopted. The wave propagation in cardiac tissue was computed using the monodomain method implemented

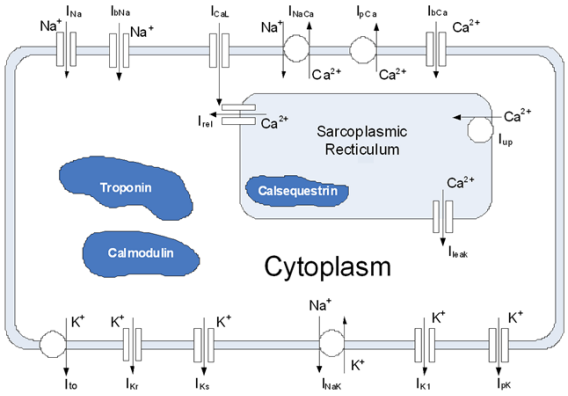

Fig. 1. A schematic of the human ventricular cell model adopted from ten Tusscher *et al.* [20]. Here, I_{Na} is the fast Na^+ current, I_{K1} is the inward rectifier K^+ current, I_{to} is the transient outward current, I_{Kr} is the rapid delayed rectifier current, I_{Ks} is the slow delayed rectifier current, I_{CaL} is the L-type Ca^{2+} current, I_{NaCa} is the Na^+/Ca^{2+} exchanger current, I_{NaK} is the Na^+/K^+ pump current, I_{pCa} and I_{pK} are the plateau Ca^{2+} and K^+ currents, respectively, I_{bCa} and I_{bK} are the respective background Ca^{2+} and K^+ currents, I_{rel} is the calcium-induced calcium release current, I_{up} is the pump current taking up calcium in the sarcoplasmic reticulum, and I_{leak} is the leakage current from the sarcoplasmic reticulum.

in a two-dimensional (2D) finite element method (FEM). To simulate fibrotic hypertrophy, we distributed cells that blocked conduction randomly throughout the computational domain to mimic the absence of gap junctions in fibroblasts. Based on previous experimental results, the electrical conductivity of fibroblasts was estimated numerically and applied to the 2D tissue model. Here, a parametric study analyzed the effect of the percentage of fibroblasts (*i.e.*, the degree of fibrosis) on the reentry pattern.

II. MATERIALS AND METHODS

1. Governing Equation of Electric Wave Propagation for 2D Cardiac Tissue

The TNNP model of a human ventricular cell proposed by ten Tusscher *et al.* [20] was used for 2D tissue modeling. A schematic of the TNNP model is shown in Fig. 1, including the ion channels, ion pumps across the cell membrane, and intracellular calcium dynamics. This includes recent experimental data on the major ionic currents, the fast Na^+, L-type Ca^{2+}, transient outward, rapid, and slow-delayed rectifier K^+ currents, as described in the original paper. We used the model without any change from the original formulation; this ventricular cell model was incorporated into the cardiac tissue model.

The cardiac tissue is divided into intracellular and interstitial spaces. Each area acts like a volume conductor that has its own volume average potential fields, current, and conductivity tensor, and the ionic currents pass from one area to another through the cell membrane. We assumed the absence of spatial variation in the electric potential inside the interstitial space and used a monodomain method [20] for the tissue model. Therefore, the governing equation of the 2D cardiac tissue model can be described by the following partial differential equation in reaction–diffusion form:

$$\frac{\partial V}{\partial t} = -\frac{I_{ion} + I_{stim}}{C_m} + \left(D_x \frac{\partial^2 V}{\partial x^2} + D_y \frac{\partial^2 V}{\partial y^2} \right), \quad (1)$$

where V is the voltage, t is the time, x and y denote the 2D Cartesian coordinates, C_m is the membrane capacitance of the ventricular cell, D_x and D_y are the diffusion coefficients of electric wave propagation in the x and the y directions, respectively, I_{stim} is the externally applied stimulus current, and I_{ion} is the sum of all transmembrane ionic currents as described in the following equation:

$$I_{ion} = I_{Na} + I_{K1} + I_{to} + I_{Kr} + I_{Ks} + I_{CaL} + I_{NaCa} + I_{NaK} + I_{pCa} + I_{pK} + I_{bCa} + I_{bNa}. \quad (2)$$

The ion currents in this equation are described in the caption of Fig. 1. A more detailed explanation of the currents is given in ten Tusscher *et al.* [20]. Since we assume an isotropic 2D tissue computation, the diffusion coefficient is $D_x = D_y$.

A forward Euler method was used for the temporal discretization of Eq. (1), and a FEM was applied for spatial discretization. A time step of $\Delta t = 0.01$ ms and a space step of $\Delta x = \Delta y = 0.02$ cm were used. The tissue measured 25×25 cm in the x and y directions, respectively. Previously, we validated this code for human cardiac tissue in our studies of 2-D and 3-D problems [21–23].

2. Initiation of a Reentrant Wave

We used the S1–S2 protocol described in Fenton *et al.* [15] to induce a reentrant wave in the tissue plane. Initially, the cells located at the boundary surface of $x = 0$ cm were stimulated, and the depolarization wave traveled in the x direction (S1 protocol). After the repolarization wave passed through the boundary surface at $x = 0$ cm, half of the depolarized domain was reset to the initial conditions to induce instability (S2 protocol). In this simulation, the S2 protocol was imposed at $t = 400$ ms. A schematic of the S1–S2 protocol in the 2D tissue model is shown in Fig. 2.

3. Estimating the Electrical Conductivity of Fibroblasts

To estimate the diffusion coefficient of the electric wave in the fibrotic tissue, we simulated a one-dimensional

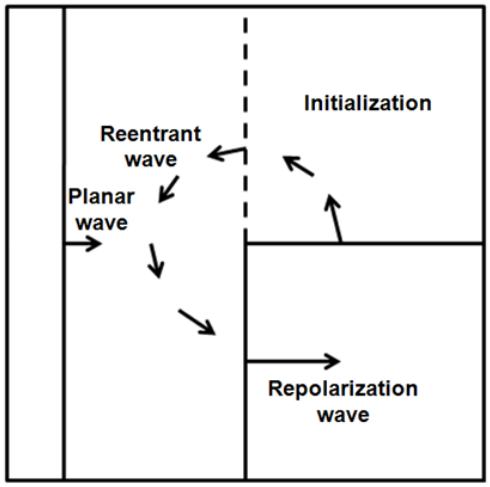

Fig. 2. Schematic of a 2D tissue model with a description of wave propagation and the S1–S2 protocol for inducing spiral waves.

(1D) model identical to the experiment of Gaudesius *et al.* [24], which measured the delay time of electric wave propagation due to fibroblasts located in the middle of a 1D array of ventricular cells. In the cell array, the cell to the far left was stimulated first and depolarized; then, the depolarization wave propagated toward the right of the cell array. When the wave met fibroblasts, the conduction of the wave was delayed significantly. The simulation was performed iteratively by varying the diffusion coefficient until the computed delay time of electric wave propagation matched that of the experiment. Then, we applied the selected value of the diffusion coefficient to the 2D fibrotic tissue model.

4. Fibrotic Tissue

Fibrosis is the pathological state in which the portion of fibroblasts in muscle tissue increases gradually with the progress of disease, eventually resulting in heart failure. Since fibroblasts are not connected electrically to other cardiac cells via gap junctions, the increased percentage of fibroblasts significantly delays the conduction of an electric wave. To simulate the effect of fibroblasts on the reentrant wave dynamics, we constructed a fibrosis model of ventricular tissue. We distributed cells that delayed conduction randomly in the computational domain to mimic the conduction delay due to fibroblasts. For the cells with delayed conduction, the diffusion coefficient of the cardiac tissue was set to the value estimated in the 1D simulation. For the parametric study to examine fibrosis of differing severity, the portion of cells with delayed conduction in the tissue was varied from 10 % to 40 % in 10 % increments. We used random number generation to distribute the cells with delayed conduction in the tissue. The S1–S2 protocol was also used to induce

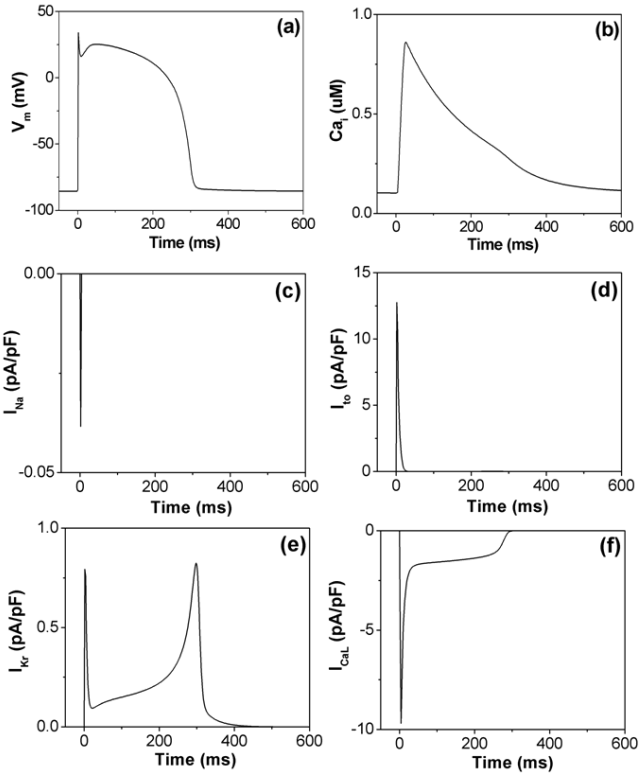

Fig. 3. Action potential, Ca^{2+} transients, and major ionic currents under 1-Hz pacing for an epicardial cell using the TNNP model: (a) action potential, V_m, (b) calcium transient, Ca_i, (c) fast sodium current, I_{Na}, (d) transient outward current, I_{to}, (e) rapid delayed rectifier current, I_{Kr}, and (f) L-type calcium current, I_{CaL}.

a reentrant wave for this fibrotic tissue. Other simulation conditions for the action potential propagation are shown in Table 1.

III. RESULTS

1. Cellular Model

First, we present the cellular results using the TNNP model. The shapes of the action potential, Ca^{2+} transient, and major ionic currents were reconstructed well for a 1.0-s cardiac cycle (Fig. 3). The action potential had the characteristic spike-notch-dome shape of human cardiac cells with a resting potential of –87.3 mV. The maximum plateau potential was +21.7 mV, and the duration of the action potential at 90 % repolarization was approximately 265 ms (Fig. 3(a)). The calcium transient had the characteristic rounded-off triangular shape, the diastolic Ca^{2+} level was 0.07 μM, and the maximum systolic calcium level was 0.9 μM (Fig. 3(b)). The sodium channel was opened abruptly by the action potential, and sodium ions flowed into the intracellular

Table 1. Conditions for simulating propagation of the action potential through ventricular tissue.

Simulation conditions	Values	References
Diffusion coefficient	0.00154 cm^2/ms	ten Tusscher *et al.* [20]
Cell capacitance per unit surface area	$C_m = 2\ \mu F/cm^2$	ten Tusscher *et al.* [20]
Time-step size	0.01 ms	Model parameter
Space-step size	0.01 cm	Model parameter
Initial values of the model variables		
Action potential baseline value	–87.3 mV	ten Tusscher *et al.* [20]
Intracellular Ca^{2+} concentration	0.2 μM	ten Tusscher *et al.* [20]
Stimulus conditions		
Stimulus magnitude	50 pA/pF	Model parameter
Stimulus duration	1 ms	Model parameter

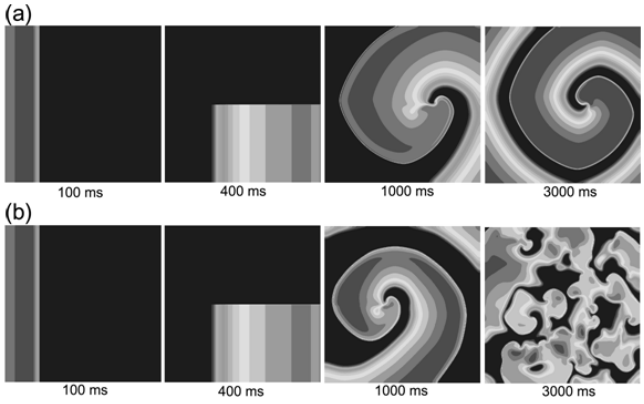

Fig. 4. Sequential contours of action potential propagation for a reentrant wave in (a) normal and (b) pathological cardiac tissues based on the action potential duration restitution hypothesis: t = 100, 400, 1000, and 3000 ms.

cytoplasm, which induced inward current. However, it then closed immediately, showing a peak current during the initial stage of depolarization (Fig. 3(c)). If the membrane potential increases to a saturated value, the potassium channels are open to repolarize the potential, inducing outward currents I_{to} and I_{Kr} (Figs. 3(d) and 3(e)). The L-type calcium channel opens when the membrane potential depolarizes, so the inward current increases abruptly. Subsequently, it maintains a constant value during the plateau potential (Fig. 3(f)). These findings were similar to the original results obtained by using the TNNP model [20].

2. 2D Tissue Baseline Model

Figure 4 shows the sequential plots of the action potential contour for generating a reentrant wave by using the S1–S2 protocol. The depolarization wave traveled in the x direction. The repolarization wave passing through the midplane is plotted at 400 ms when the S2 protocol was applied to the wave. The sharp edge formed by the S1–S2 protocol near the center of the computational domain induced instability of the traveling wave and generated a spiral wave. The 2D simulations were performed on a 1250 × 1250 square lattice of epicardial ventricular cells.

In normal cardiac tissue, the reentrant wave remained stable and did not lead to ventricular fibrillation. In pathological cardiac tissue, for which the cellular characteristics are given in ten Tusscher *et al.* [17], for the action potential duration restitution hypothesis, the maximum conductances of I_{Kr} (G_{Kr}) and I_{Ks}(G_{Ks}) were set to values 12 % higher than normal. The maximum conductances of I_{pCa} (G_{pCa}) and I_{pK}(G_{pK}) were set to 7 times higher and 85 % lower than normal values, respectively. The time constant of the f gate in the I_{CaL} channel was set to 2 times higher than normal. Spiral breakup occurred, and ventricular fibrillation ultimately developed [Fig. 4(b)].

3. 2D Fibrotic Tissue Model

Figure 5(a) shows a phase-contrast image of an 80-μm-wide strand of cardiomyocytes with a central fibroblast and the measured activation time of cellular excitation according to the distance from the left side of the region in the experiment of Gaudesius *et al.* [24]. A significant delay in the activation time due to fibroblasts was observed after the region containing fibroblasts. Figure 5(b) shows the activation time determined for various electrical conductivities in the fibroblast region. As the electrical conductivity of the fibroblasts decreased, the activation delay time increased gradually. For a conductivity value of $D_{fibro} = D_{normal}/85$, the conduction delay time was closest to the experimental value (30 ms). Therefore, we chose $D_{fibro} = D_{normal}/85$ as the conductivity of the fibroblast region for our 2D model.

To analyze the effect of the severity of fibrosis on reentrant dynamics, we first initiated a reentrant wave and then gradually increased the severity of fibrosis. Figure 6 shows the temporal variation in the action potential

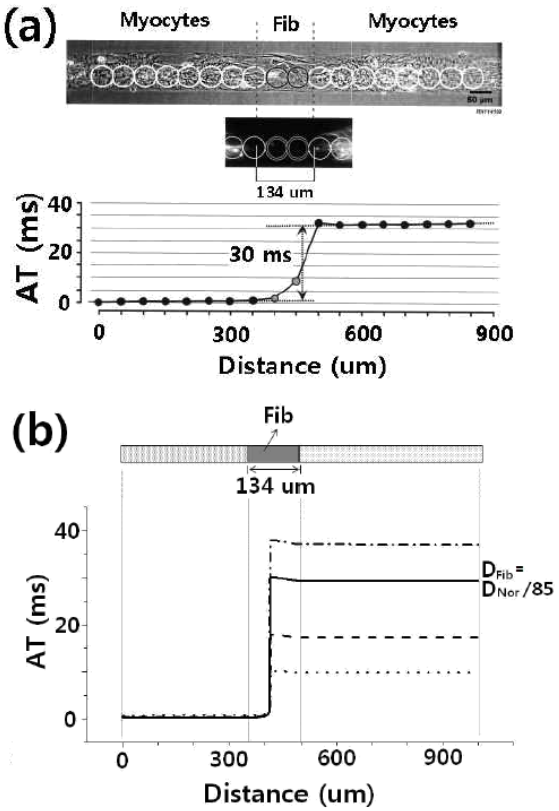

Fig. 5. Cellular activation times obtained from the experiment and the simulation. (a) Phase-contrast image of an 80-μm-wide strand of cardiomyocytes with a central fibroblast [top] and the measured activation time along the strand [bottom] (adopted from Gaudesius *et al.* [24]). (b) Computed activation time along the simulated strand of single cells according to the electrical conductivity of the fibroblast. Fib indicates fibroblasts, Nor indicates normal.

contours of the reentrant wave according to the severity of fibrosis. The four columns represent the times elapsed since initiation of the reentrant wave (2, 4, 6, and 8 seconds). The four rows represent different percentages of fibroblasts (10, 20, 30, and 40 % fibroblasts). In comparison with the reentrant wave in normal cardiac tissue without fibrosis [Fig. 4(a)], fibrotic tissues showed many discontinuities of the action potential wave. Although a partial conduction delay was observed for 10 % and 20 % fibrosis, and a greater conduction delay was observed for 30 % fibrosis, ventricular fibrillation was not induced. With 40 % fibrosis, the conduction delay was greater, and the single reentrant wave broke into multiple waves, eventually resulting in ventricular fibrillation after 4 s. Although the cellular characteristics of the fibrotic tissue were set to normal, the 40 % fibrotic tissue, similar to pathological cardiac tissue, developed spiral breakup and ultimately, ventricular fibrillation. This indicates that electric instability of tissue and ventricular fibrillation can occur, depending on extracellular characteristics, even without cellular perturbation.

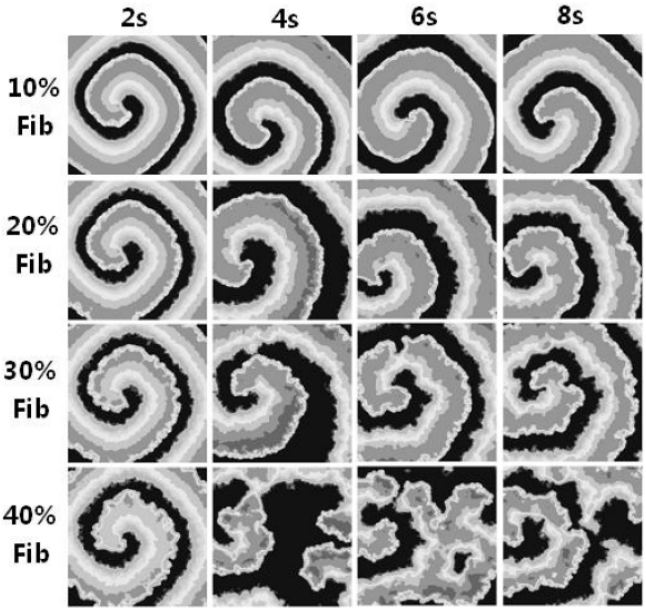

Fig. 6. Sequential contours of the action potential in the fibrotic tissue model according to the percentage of fibroblasts (10 %, 20 %, 30 %, and 40 %). Fib indicates fibroblasts.

IV. DISCUSSION

In this study, we delineated the effect of the severity of fibrosis on reentrant wave dynamics by using a computational model that consisted of an electrophysiological model of 2D ventricular tissue based on an existing cellular model and the monodomain method implemented in a 2D FEM. Using the TNNP model, the typical shape of the cellular action potential was reproduced well, showing the spike-notch-dome-style pattern of a human ventricular cell. In addition, the calcium dynamics and major ionic current profiles matched with original results of ten Tusscher *et al.* [20] and the experimental results [25,26] well (Fig. 3). The reentrant wave propagation resulted in a single, focused, regular reentrant wave in normal cardiac tissue [Fig. 4(a)], but it showed spiral breakup and developed ventricular fibrillation when cellular pathology was present [Fig. 4(b)]. To test the reentrant wave dynamics in fibrosis, we simulated fibrotic tissue containing a defined proportion of fibroblasts among the tissue cells by using a stochastic method. The conductivity of fibroblasts in the tissue model was estimated from iterative simulations of a 1D model mimicking a previous experiment (Fig. 5). Compared to normal tissue, the fibrotic tissue resulted in a partial conduction delay and the single reentrant wave was broken into multiple waves at a fibrosis severity of 40 %, eventually causing ventricular fibrillation (Fig. 6).

Fibrotic tissue is a recognized source of instability, capable of breaking a single focused reentrant wave into multiple waves [27]. Although this has been observed experimentally, no quantitative or theoretical study of

the phenomenon had been carried out. The main contribution of this paper to this field is that it provides quantitative results for the effect of fibrosis on reentrant waves. Analyzing the effect of fibrosis on reentrant wave stability experimentally is difficult due to the lack of a precise voltage measuring device, along with problems in varying the severity of fibrosis experimentally. Note that the simulation with a fibrosis severity of 40 % resulted in an irregular reentrant wave pattern with multiple foci. The finding that a greater delay in wave propagation at a greater severity of fibrosis resulted in a marked increase in the probability of chaotic waves forming provides further *in silico* evidence for the physiological impact of fibrosis severity on reentrant wave dynamics.

ACKNOWLEDGMENTS

This study was supported in part by IITA through IT Leading R & D Support Project, by the ITRC Grid middleware center, by the Korea Research Foundation Grant funded by the Korean Government (MEST) (The Regional Research Universities Program/Medical & Bio-Materials Research Center).

REFERENCES

[1] C. N. D'Alnoncourt, W. Zierhut and B. Bluderitz, Br Heart J **48**, 213 (1982).
[2] L. M. Rodriguez, E. B. Sternick, J. L. Smeets, C. Timmermans, K. den Dulk, G. Oreto and H. J. Wellens, Heart (British Cardiac Society) **75**, 23 (1996).
[3] W. A. Schaffer and L. A. Cobb, The New England Journal of Medicine **293**, 259 (1975).
[4] J. M. Cao, Z. Qu, Y. H. Kim, T. J. Wu, A. Garfinkel, J. N. Weiss, H. S. Karagueuzian and P. S. Chen, Circ Res **84**, 1318 (1999).
[5] E. Cytrynbaum and J. P. Keener, Chaos **12**, 788 (2002).
[6] J. J. Fox, E. Bodenschatz and R. F. Gilmour, Jr., Phys. Rev. Lett. **89**, 138101 (2002).
[7] N. F. Otani and R. F. Gilmour, Jr., J Theor Biol **187**, 409 (1997).
[8] Z. Qu, J. N. Weiss and A. Garfinkel, Am J Physiol **276**, H269 (1999).
[9] E. G. Tolkacheva, D. G. Schaeffer, D. J. Gauthier and W. Krassowska, Phys. Rev. E Stat. Nonlin Soft Matter Phys **67**, 031904 (2003).
[10] E. M. Cherry and F. H. Fenton, Am J Physiol Heart Circ Physiol **286**, H2332 (2004).
[11] A. Karma, Chaos **4**, 461 (1994).
[12] K. Gima and Y. Rudy, Circ Res **90**, 889 (2002)
[13] Y. Rudy, Ann Biomed Eng **28**, 945 (2000).
[14] F. Xie, Z. Qu, J. Yang, A. Baher, J. N. Weiss and A. Garfinkel, J Clin Invest **113**, 686 (2004).
[15] F. H. Fenton, E. M. Cherry, H. M. Hastings and S. J. Evans, Chaos **12**, 852 (2002).
[16] O. Berenfeld and J. Jalife, Circ Res **82**, 1063 (1998).
[17] K. H. ten Tusscher and A. V. Panfilov, Am J Physiol Heart Circ Physiol **291**, H1088 (2006).
[18] M. G. Nicholls, Heart (British Cardiac Society) **76**, 92 (1996).
[19] G. R. Norton, A. J. Woodiwiss, W. H. Gaasch, T. Mela, E. S. Chung, G. P. Aurigemma and T. E. Meyer, Journal of the American College of Cardiology **39**, 664 (2002).
[20] K. H. ten Tusscher, D. Noble, P. J. Noble and A. V. Panfilov, Am J Physiol Heart Circ Physiol **286**, H1573 (2004).
[21] U. B. Im, S. S. Kwon, K. Kim, Y. H. Lee, Y. K. Park, C. H. Youn and E. B. Shim, Prog Biophys Mol Biol **96**, 339 (2008).
[22] U. B. Im, E. B. Shim, K. Kim, Y. H. Lee and Y. K. Park, J Korean Phys. Soc. **50**, 78 (2007).
[23] E. B. Shim, C. H. Leem, Y. Abe and A. Noma, Philos Transact A Math Phys Eng Sci **364**, 1483 (2006).
[24] G. Gaudesius, M. Miragoli, S. P. Thomas and S. Rohr, Circ Res **93**, 421 (2003).
[25] G. A. Gintant, Am J Physiol Heart Circ Physiol **278**, H806 (2000).
[26] Z. Zhou, Q. Gong, B. Ye, Z. Fan, J. C. Makielski, G. A. Robertson and C. T. January, Biophys J **74**, 230 (1998).
[27] T. J. Wu, J. J. Ong, C. Hwang, J. J. Lee, M. C. Fishbein, L. Czer, A. Trento, C. Blanche, R. M. Kass, W. J. Mandel, H. S. Karagueuzian and P. S. Chen, Journal of the American College of Cardiology **32**, 187 (1998).